

Sensing Mutual Information with Random Signals in Gaussian Channels

Lei Xie^{*}, Fan Liu[†], Zhanyuan Xie[‡], Zheng Jiang[‡], and Shenghui Song^{*}

^{*}The Hong Kong University of Science and Technology, Hong Kong

[†]Southern University of Science and Technology, China

[‡]China Telecom Research Institute, China

Abstract—Sensing performance is typically evaluated by classical metrics, such as Cramér-Rao bound and signal-to-clutter-plus-noise ratio. The recent development of the integrated sensing and communication (ISAC) framework motivated the efforts to unify the metric for sensing and communication, where researchers have proposed to utilize mutual information (MI) to measure the sensing performance with deterministic signals. However, the need to communicate in ISAC systems necessitates the use of random signals for sensing applications and the closed-form evaluation for the sensing mutual information (SMI) with random signals is not yet available in the literature. This paper investigates the achievable performance and precoder design for sensing applications with random signals. For that purpose, we first derive the closed-form expression for the SMI with random signals by utilizing random matrix theory. The result reveals some interesting physical insights regarding the relation between the SMI with deterministic and random signals. The derived SMI is then utilized to optimize the precoder by leveraging a manifold-based optimization approach. The effectiveness of the proposed methods is validated by simulation results.

Index Terms—Integrated sensing and communication, sensing mutual information, random signal, sensing degree of freedom, precoder design.

I. INTRODUCTION

With the development of innovative applications that demand accurate environment information, e.g., autonomous driving and unmanned aerial vehicle (UAV) networks, sensing becomes an essential requirement for future wireless networks. To this end, the integrated sensing and communications (ISAC) framework has attracted much attention [1], [2]. However, there are still substantial challenges that need to be tackled before we can fully unleash the potential of ISAC. For example, sensing and communication systems have been developed separately for many years with their own performance metrics. In particular, sensing performance is normally characterized by metrics such as Cramér-Rao bound (CRB) [3], signal-to-clutter-plus-noise ratio [4], and minimum mean-square error [5], while communication performance is usually measured by mutual information (MI) [6] and outage probability [7]. The inconsistency between the performance metrics of two systems poses challenges to integrative design.

Recently, some research efforts have been devoted to unifying the performance metric for sensing and communication. For that purpose, MI has been utilized to measure sensing performance [8]–[12]. For example, the authors of [10] showed that the radar waveform that maximizes the MI between the

Gaussian-distributed target response and the received signal also minimizes the MMSE for estimating the target response. However, existing works [8]–[10] mainly focused on the sensing MI (SMI) with deterministic signals, and the result is not applicable to ISAC systems that utilize random signals for joint sensing and communication purposes. Recently, some works considered the sensing performance with random signals and revealed the intrinsic connection between SMI and other metrics from a rate-distortion perspective [11], [12]. However, a closed-form expression for the SMI of systems utilizing random signals is not yet available.

This paper has two objectives: 1) to evaluate the sensing performance with random signals; and 2) to optimize the sensing performance through signal design. To achieve the first objective, we derive a closed-form expression for the SMI between the random target response and the received signals, where random signals are utilized. It is shown that the SMI with random signals is upper-bounded by that with a properly-designed deterministic signal. The performance loss due to the use of random signals is also investigated. Building upon the theoretical result, we maximize the SMI by optimizing the transmit signal with manifold optimization. Simulation results show that the proposed method achieves superior performance than existing methods.

The remainder of the paper is organized as follows. Section II presents the system model. Section III provides a closed-form expression for the SMI and reveals some physical insights. Section IV introduces a manifold-based approach to maximize the SMI by optimizing the transmitted precoder. Simulation results are given in Section V to validate the effectiveness of the proposed manifold-based method. Finally, Section V concludes the paper, summarizing the key findings and contributions.

II. SYSTEM MODEL

Consider a bi-static sensing system, which is composed of a sensing transmitter equipped with N_T antennas and a sensing receiver with N_R antennas. Assume that the target sensing is performed within a coherent processing interval (CPI) consisting of N_S frames. The baseband received signal in a CPI is given by [9]

$$\mathbf{Y} = \mathbf{H}\mathbf{X} + \mathbf{N} \in \mathcal{C}^{N_R \times N_S}, \quad (1)$$

where $\mathbf{X} \in \mathcal{C}^{N_T \times N_S}$ denotes the transmitted signal, \mathbf{H} represents the target response matrix, and $\mathbf{N} \in \mathcal{C}^{N_R \times N_S}$ is the additive white Gaussian noise. The target response matrix can be given by

$$\mathbf{H} = \sum_{k=1}^K \epsilon_k \mathbf{b}(\vartheta_k) \mathbf{a}^H(\phi_k) \in \mathcal{C}^{N_R \times N_T} \quad (2)$$

where K denotes the number of sensing targets. Note that ϵ_k represents the complex reflection coefficient of the k th target and its amplitude is determined by the path loss and the radar cross section (RCS). The reflection coefficient is normally assumed to follow Gaussian distribution with $\epsilon_k \sim \mathcal{CN}(0, \sigma_k^2)$. The two vectors, i.e., $\mathbf{a}(\cdot)$ and $\mathbf{b}(\cdot)$, denote the steering vectors for the transmit and receive array, respectively, and ϑ_k and ϕ_k represent the angle of departure (AOD) and the angle of arrival (AOA) for the k th target, respectively.

Different from conventional radar systems which typically use deterministic signal, ISAC systems use random signals for communication purposes. In this paper, we consider the widely adopted Gaussian signal with $\mathbf{X} = \mathbf{F}\mathbf{S}$, where $\mathbf{F} \in \mathcal{C}^{N_T \times K}$ represents the precoder matrix and $\mathbf{S} \in \mathcal{C}^{K \times N_S}$ denotes a random matrix whose entries are independent and identically distributed (i.i.d.) Gaussian random variables with variance $\frac{1}{N_S}$ and $N_S \geq K$. It follows that $\mathbb{E}(\mathbf{S}\mathbf{S}^H) = \mathbf{I}$. By stacking the columns of \mathbf{Y}^H , we can obtain

$$\mathbf{y} \triangleq \text{vec}(\mathbf{Y}^H) = \hat{\mathbf{X}}^H \mathbf{h} + \mathbf{n} \in \mathcal{C}^{N \times 1}, \quad (3)$$

where $N = N_T N_R$, $\hat{\mathbf{X}} = \mathbf{I}_{N_R} \otimes \mathbf{X}$, $\mathbf{h} = \text{vec}(\mathbf{H}^H)$, and $\mathbf{n} = \text{vec}(\mathbf{N}^H) \sim \mathcal{CN}(\mathbf{0}, \sigma_N^2 \mathbf{I}_N)$. The channel correlation matrix $\mathbf{R} \triangleq \mathbb{E}(\mathbf{h}\mathbf{h}^H)$ can be well approximated by $\mathbf{R} = \mathbf{R}_R \otimes \mathbf{R}_T$ [13]–[15], where \mathbf{R}_R and \mathbf{R}_T denote the correlation matrices at the receiver and the transmitter, respectively, with $\text{rank}(\mathbf{R}_R) \leq K$ and $\text{rank}(\mathbf{R}_T) \leq K$. In this paper, we assume \mathbf{R}_R and \mathbf{R}_T are available to the transmitter. This assumption is justified in ISAC systems, where the prior knowledge of the targets can be obtained from previous estimates [5], [9].

III. SENSING MUTUAL INFORMATION

To detect the target, the sensing receiver will estimate the target response vector \mathbf{h} based on the received signals \mathbf{y} , or \mathbf{H} based on \mathbf{Y} , equivalently [9], [16]. Assuming a deterministic sensing signal, previous works focused on optimizing \mathbf{S} to maximize the SMI between the received signals and the target response [9], [10]. Unfortunately, such methods are no longer valid for ISAC systems when random signals are utilized. Define $\boldsymbol{\eta}$ as the parameters of interest (POI) of the targets, e.g., AOA, AOD and reflection coefficients. We assume $\boldsymbol{\eta}$ remains constant in one CPI and varies between CPIs. Any estimator for $\boldsymbol{\eta}$ aims to estimate a particular realization of $\boldsymbol{\eta}$ within one CPI. Note that $\boldsymbol{\eta}$ captures all uncertainty of \mathbf{H} , and when \mathbf{H} is an injective map of $\boldsymbol{\eta}$, the MI between $\boldsymbol{\eta}$ and the received signals \mathbf{y} is equivalent to that between \mathbf{h} and \mathbf{y} , i.e., $I(\boldsymbol{\eta}; \mathbf{y}|\mathbf{S}) = I(\mathbf{h}; \mathbf{y}|\mathbf{S})$ [11].

For ease of evaluation, we assume that \mathbf{h} follows a Gaussian distribution, i.e., $\mathbf{h} \sim \mathcal{CN}(\mathbf{0}, \mathbf{R})$, which has been widely

adopted for MIMO channel [15] and target response matrix [9]–[11]. Under such circumstances, the SMI with random signals is defined as

$$\begin{aligned} I_G(\boldsymbol{\eta}; \mathbf{y}|\mathbf{S}) &= I_G(\mathbf{h}; \mathbf{y}|\mathbf{S}) \\ &\triangleq \mathbb{E}_{\mathbf{S}} \log \left| \mathbf{I} + \sigma_N^{-2} \left(\mathbf{R}_R \otimes \mathbf{R}_T^{\frac{1}{2}} \mathbf{F} \mathbf{S} \mathbf{S}^H \mathbf{F}^H \mathbf{R}_T^{\frac{1}{2}} \right) \right|, \end{aligned} \quad (4)$$

where the expectation is taken over the random signals \mathbf{S} . Note that $I_G(\boldsymbol{\eta}; \mathbf{y}|\mathbf{S})$ represents the highest SMI that can be achieved. Additionally, according to [11], SMI is directly related to the distortion metric (e.g., the estimation error) of $\boldsymbol{\eta}$. Unfortunately, the expectation in (4) is computationally prohibitive due to the high-dimensional integrals.

A. Upper bound of SMI

An upper bound of SMI can be obtained by applying the Jensen's inequality on (4). In particular, we have

$$I_G(\boldsymbol{\eta}; \mathbf{y}|\mathbf{S}) \leq \log \left| \mathbf{I} + \sigma_N^{-2} \left(\mathbf{R}_R \otimes \mathbf{R}_T^{\frac{1}{2}} \mathbf{F} \mathbb{E}_{\mathbf{S}}(\mathbf{S}\mathbf{S}^H) \mathbf{F}^H \mathbf{R}_T^{\frac{1}{2}} \right) \right|,$$

where the equality holds when $\mathbf{S}\mathbf{S}^H = \mathbf{I}$. Thus, we can obtain the upper bound as

$$\tilde{I}_G(\boldsymbol{\eta}; \mathbf{y}) \triangleq \log \left| \mathbf{I} + \sigma_N^{-2} \left(\mathbf{R}_R \otimes \mathbf{R}_T^{\frac{1}{2}} \mathbf{F} \mathbf{F}^H \mathbf{R}_T^{\frac{1}{2}} \right) \right|. \quad (5)$$

Thus, there are two ways to interpret $\tilde{I}_G(\boldsymbol{\eta}; \mathbf{y})$. On the one hand, $\tilde{I}_G(\boldsymbol{\eta}; \mathbf{y})$ can be regarded as the MI obtained by a deterministic signal with sample covariance matrix \mathbf{I} . On the other hand, as an upper bound, $\tilde{I}_G(\boldsymbol{\eta}; \mathbf{y})$ can be utilized as an approximation for SMI when N_S is large. This is because, as $N_S \rightarrow \infty$, the sample covariance matrix $\mathbf{S}\mathbf{S}^H$ will tend to be deterministic, i.e., $\lim_{N_S \rightarrow \infty} \mathbf{S}\mathbf{S}^H \rightarrow \mathbf{I}$. Under such circumstances, $I_G(\boldsymbol{\eta}; \mathbf{y}|\mathbf{S})$ approaches its upper bound $\tilde{I}_G(\boldsymbol{\eta}; \mathbf{y})$. Unfortunately, as we will show later, the precision of this approximation is poor when N_S is small.

B. Asymptotic approximation of SMI

In this paper, we derive a closed-form expression for the SMI by analyzing the asymptotic behavior of $I_G(\mathbf{h}; \mathbf{y})$. In particular, we provide an approximation for the SMI in the large N_S regime based on the first order approximation of the MI. The result is shown in the following proposition.

Proposition 1: As $N_S, K \rightarrow \infty$ with a finite constant ratio c , i.e., $N_S/K = c$, we have

$$I_G(\boldsymbol{\eta}; \mathbf{y}|\mathbf{S}) = \sum_{j=1}^K \bar{q}_j(\mathbf{F}) + \mathcal{O}\left(\frac{1}{N_S}\right), \quad (6)$$

where

$$\begin{aligned} \bar{q}_j(\mathbf{F}) &= \log \left| \mathbf{I}_{N_T} + \frac{\lambda_{R,j}}{1 + \lambda_{R,j} \delta(\lambda_{R,j})} \mathbf{T}(\mathbf{F}) \right| \\ &+ N_S \log(1 + \lambda_{R,j} \delta(\lambda_{R,j})) - N_S \frac{\lambda_{R,j} \delta(\lambda_{R,j})}{1 + \lambda_{R,j} \delta(\lambda_{R,j})}, \end{aligned} \quad (7)$$

with $\mathbf{T}(\mathbf{F}) \triangleq \mathbf{R}_T^{\frac{1}{2}} \mathbf{F} \mathbf{F}^H \mathbf{R}_T^{\frac{1}{2}}$. $\{\lambda_{R,j}\}_{j=1}^K$ denotes the eigenvalues of $\sigma_N^{-2} \mathbf{R}_R$, and $\delta(\rho)$ is the solution to the following equation

$$\delta(\rho) = \frac{1}{N_S} \text{tr} \mathbf{T}(\mathbf{F}) \left(\mathbf{I}_{N_T} + \frac{\rho}{1 + \rho \delta(\rho)} \mathbf{T}(\mathbf{F}) \right)^{-1}. \quad (8)$$

Proof: See Appendix A. ■

Proposition 1 provides a closed-form expression for the SMI between the POI and the received signals. Note that, different from the upper bound in (5), *Proposition 1* aims to approximate SMI by analyzing its asymptotic behavior. As will be shown later, although (6) is derived under the condition that N_S and K approach infinity, it provides accurate approximation for SMI even when N_S and K are small.

C. Effect of the number of frames

With the explicit expression for the SMI, we can evaluate the impact of key system parameters. To evaluate the effect of N_S , we calculate the derivative of the SMI with respect to N_S . First, for all $N_S \geq 0$, the derivative of $\bar{q}_j(\mathbf{F})$, which is given in (7), with respect to N_S can be given by

$$\begin{aligned} \frac{\partial \bar{q}_j}{\partial N_S} &= -\frac{\lambda_{R,j}^2 \text{tr} \mathbf{T} \left(\mathbf{I}_{N_T} + \frac{\lambda_{R,j}}{1 + \lambda_{R,j} \delta(\lambda_{R,j})} \mathbf{T} \right)^{-1}}{(1 + \lambda_{R,j} \delta(\lambda_{R,j}))^2} \\ &+ \frac{N_S \lambda_{R,j}}{1 + \lambda_{R,j} \delta(\lambda_{R,j})} - \frac{N_S \lambda_{R,j}}{(1 + \lambda_{R,j} \delta(\lambda_{R,j}))^2} \\ &+ \log(1 + \lambda_{R,j} \delta(\lambda_{R,j})) - \frac{\lambda_{R,j} \delta(\lambda_{R,j})}{1 + \lambda_{R,j} \delta(\lambda_{R,j})} \\ &\stackrel{(a)}{=} \log(1 + \lambda_{R,j} \delta(\lambda_{R,j})) - \frac{\lambda_{R,j} \delta(\lambda_{R,j})}{1 + \lambda_{R,j} \delta(\lambda_{R,j})} \geq 0, \end{aligned} \quad (9)$$

where step (a) follows (8). Thus, we have

$$\frac{\partial I_G(\boldsymbol{\eta}; \mathbf{y}|\mathbf{S})}{\partial N_S} = \sum_{j=1}^K \frac{\partial \bar{q}_j}{\partial N_S} \geq 0. \quad (10)$$

This indicates that the SMI $I_G(\boldsymbol{\eta}; \mathbf{y}|\mathbf{S})$ is monotonically increasing with respect to N_S .

D. Sensing DoF loss

To measure the impact of random signals on sensing, we further investigate the sensing Degree of Freedom (DoF). This concept was introduced in [17] to measure the loss of CRB induced by the random signals and defined as the effective number of independent observations. By following the same idea, we define the SMI-oriented sensing DoF as

$$\nu_s = \lim_{\sigma_N^2 \rightarrow 0} \frac{N_S I_G(\boldsymbol{\eta}; \mathbf{y}|\mathbf{S})}{\tilde{I}_G(\boldsymbol{\eta}; \mathbf{y}|\mathbf{S})}. \quad (11)$$

where the maximum sensing DoF is the total number of the independent observations N_S . The normalization coefficient $\frac{I_G(\mathbf{h}; \mathbf{y})}{\tilde{I}_G(\mathbf{h}; \mathbf{y})}$ is the ratio between the SMI with random signals and its upper bound achieved by deterministic signals. Thus, this ratio measures the MI loss caused by the randomness of signals. The following proposition provides the lower bound for $I_G(\boldsymbol{\eta}; \mathbf{y}|\mathbf{S})$, based on which the maximum sensing DoF loss can be obtained.

Proposition 2: When $N_S \geq K$, we have

$$I_G(\boldsymbol{\eta}; \mathbf{y}|\mathbf{S}) \geq \frac{N_S - \min\{K, \text{rank}(\mathbf{F}\mathbf{F}^H)\}}{N_S} \tilde{I}_G(\boldsymbol{\eta}; \mathbf{y}|\mathbf{S}). \quad (12)$$

Proof: See Appendix B. ■

Based on *Proposition 2*, the sensing DoF can be bounded by

$$N_S - \min\{K, \text{rank}(\mathbf{F}\mathbf{F}^H)\} \leq \nu_s \leq N_S. \quad (13)$$

This indicates that $\min\{K, \text{rank}(\mathbf{F}\mathbf{F}^H)\}$ is the maximum sensing DoF loss defined based on SMI, which coincides with the sensing DoF loss defined based on CRB [17]. It can be observed that maximum sensing DoF loss will increase with K . This is because the system needs to separate the signals associated with different targets, and this task becomes more challenging as the number of targets increases, due to the interference between different targets. As a result, more samples are required to mitigate such a loss. In particular, according to the squeeze theorem, there is no loss when $N_S \rightarrow \infty$, because the lower bound of $I_G(\boldsymbol{\eta}; \mathbf{y}|\mathbf{S})$ in (12) approaches $\tilde{I}_G(\boldsymbol{\eta}; \mathbf{y}|\mathbf{S})$. This agrees with the theoretical results in (10).

IV. SMI-ORIENTED PRECODING DESIGN

Next, we will optimize the precoder to maximize the SMI. The optimization problem is formulated as

$$\mathcal{P}_0: \max_{\mathbf{F}} \mathcal{L}(\mathbf{F}) \quad \text{s.t.} \quad \|\mathbf{F}\|^2 \leq P, \quad (14)$$

where $\mathcal{L}(\mathbf{F}) = \sum_{j=1}^K \bar{q}_j(\mathbf{F})$ and the transmit power is constrained to a maximum value of P . A common practice to solve \mathcal{P}_0 is to utilize the interior point method associated with the Newton's method, which requires both gradient and Hessian matrix. However, since δ is obtained by solving the equation defined in (8), it is difficult to obtain the Hessian matrix of $\mathcal{L}(\mathbf{F})$ with respect to \mathbf{F} . To address this issue, we propose to solve the problem \mathcal{P}_0 by exploiting the manifold steepest descent method, which makes it easier to deal with the constraint and only requires the gradient.

The manifold-based method updates the variable within the tangent space. By updating along the tangent space with a small enough step, the new point is almost within the manifold. The manifold steepest descent method requires the Euclidean gradient, the Riemannian gradient, and the projections on the manifold.

1) *Euclidean Gradient:* Define $\nabla_{\mathbf{F}} \mathcal{L}(\mathbf{F})$ as the Euclidean gradient of the objective function in (14) with respect to \mathbf{F} , which is computed as $\nabla_{\mathbf{F}} \mathcal{L}(\mathbf{F}) = \sum_{j=1}^K \nabla_{\mathbf{F}} \bar{q}_j(\mathbf{F})$, with $\nabla_{\mathbf{F}} \bar{q}_j(\mathbf{F})$ denoting the Euclidean gradient of $\bar{q}_j(\mathbf{F})$ with respect to \mathbf{F} . Note that δ defined in (8) is dependent on \mathbf{F} , which makes the derivative more complex. To this end, we first give the following lemma for obtaining the derivatives of $\delta(\rho)$ with respect to \mathbf{F} .

Proposition 3: Define $\alpha(\rho) = \frac{\rho}{1 + \rho \delta(\rho)}$. Then, the gradient of $\delta(\rho)$ with respect to \mathbf{F} , i.e., $\Delta'_\rho \triangleq \frac{\partial \delta(\rho)}{\partial \mathbf{F}^*}$ is obtained by

$$\Delta'_\rho = \frac{\mathbf{R}_T^{\frac{1}{2}} (\mathbf{I} + \alpha(\rho) \mathbf{T}(\mathbf{F}))^{-2} \mathbf{R}_T^{\frac{1}{2}} \mathbf{F}}{N_S - \alpha^2(\rho) \text{tr} \left(\mathbf{T}(\mathbf{F}) (\mathbf{I} + \alpha(\rho) \mathbf{T}(\mathbf{F}))^{-1} \right)}. \quad (15)$$

Proof: See Appendix C. ■

Based on *Proposition 3*, $\nabla_{\mathbf{F}} \bar{\varrho}_j(\mathbf{F})$ can be obtained by¹

$$\begin{aligned} \nabla_{\mathbf{F}} \bar{\varrho}_j(\mathbf{F}) &= \alpha_j^2 \text{tr}(\mathbf{M}_{T,j} \mathbf{T}) \Delta'_{\lambda_{R,j}} + \alpha_j \text{tr}(\mathbf{M}_{T,j}) \mathbf{R}_T \mathbf{F} \\ &+ N_S \alpha_j \Delta'_{\lambda_{R,j}} - \frac{N_S}{(1 + \lambda_{R,j} \delta(\lambda_{R,j}))^2} \Delta'_{\lambda_{R,j}}, \end{aligned} \quad (16)$$

where $\alpha_j(\mathbf{F}) = \alpha(\lambda_{R,j})$ and

$$\mathbf{M}_{T,j}(\mathbf{F}) = \left(\mathbf{I}_{N_S} + \alpha_j(\mathbf{F}) \mathbf{R}_T^{\frac{1}{2}} \mathbf{F} \mathbf{F}^H \mathbf{R}_T^{\frac{1}{2}} \right)^{-1}. \quad (17)$$

2) *Riemannian Gradient on Manifold*: For the manifold $\mathcal{M}_{\mathbf{F}} = \left\{ \mathbf{F} \in \mathcal{C}^{K \times N_S} \mid \|\mathbf{F}\|^2 = P \right\}$, the Riemannian gradient of $\mathcal{L}(\mathbf{F} | \mathbf{v}_k, \mathbf{Z}_k)$ at $\mathbf{F} \in \mathcal{M}_{\mathbf{F}}$ is given by [4]

$$\text{grad}_{\mathbf{F}} \mathcal{L}(\mathbf{F}) = \nabla_{\mathbf{F}} \mathcal{L}(\mathbf{F}) - \left(\frac{1}{P} \text{tr} \Re(\mathbf{F} \nabla_{\mathbf{F}}^H \mathcal{L}(\mathbf{F})) \right) \mathbf{F}. \quad (18)$$

3) *Retraction*: A retraction is needed to remap the updated points from the tangent space onto the manifold. The retraction of a tangent matrix $\mathbf{D} \in T_{\mathbf{U}} \mathcal{M}_{\mathbf{F}}$ at \mathbf{F} is defined as

$$\mathcal{P}_{\mathbf{F}}(\mathbf{D}) = \frac{P}{\|\mathbf{F} + \mathbf{D}\|} (\mathbf{F} + \mathbf{D}). \quad (19)$$

To solve (14), we propose the manifold-based method summarized in **Algorithm 1**, whose convergence is guaranteed by [18, Theorem 4.3.1].

Algorithm 1 Proposed Manifold-based Method to optimize \mathbf{F}^\dagger

Input: An initial point \mathbf{F}_0 , $\mathbf{D}_0 = -\text{grad}_{\mathbf{F}} \mathcal{L}(\mathbf{F}_0)$, and $m = 0$.

Repeat

- 1) Compute β_m via the Armijo line search step [18, Definition 4.2.2].
- 2) Update $\mathbf{F}_{m+1} = \mathcal{P}_{\mathbf{F}}(-\beta_m \text{grad}_{\mathbf{F}} \mathcal{L}(\mathbf{F}_m))$ via (18) and (19).
- 3) $m \leftarrow m + 1$.

Until Convergence criterion is met.

Output: The optimal solution $\mathbf{F}^\dagger = \mathbf{F}_m$.

V. SIMULATION RESULT

In this section, we will validate the accuracy of the theoretical analysis and the effectiveness of proposed manifold-based algorithms by simulations. We consider a mmWave system operating at a carrier frequency of 28 GHz. The AOD and AOA of the targets are generated uniformly in the range $[30^\circ, 60^\circ]$. The number of antennas on the transmitter and receiver is set as $N_T = 32$ and $N_R = 16$, respectively. For the manifold optimization, we set the maximum number of iterations as 50. To terminate the iteration, the tolerance for the norm of the gradient between two iterations is 10^{-5} . The transmission power is set as $P = 30$ dBm, the noise power is $\sigma^2 = -90$ dBm, and the signal-to-noise ratios (SNR) is set as $\text{SNR} \triangleq \frac{P \sigma_k^2}{\sigma^2} = 20$ dB.

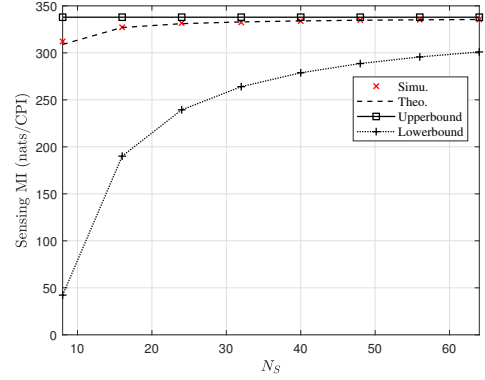


Fig. 1. Sensing MI versus the number of frames N_S .

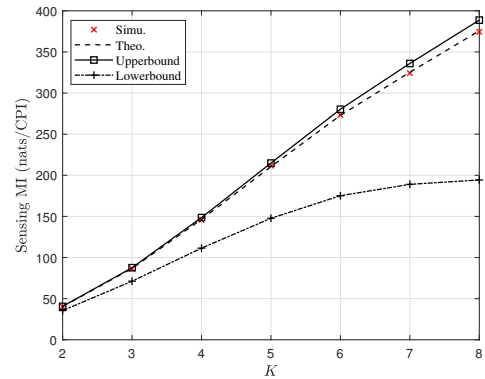


Fig. 2. Sensing MI versus the number of targets K .

A. Validation of the SMI

Fig. 1 validates the accuracy of the evaluation for SMI in *Proposition 1* with $K = 7$ targets. The legend ‘Simu.’ denotes the MI obtained by Monte-Carlo simulations, i.e., $\bar{I}(\boldsymbol{\eta}; \mathbf{y} | \mathbf{S}) = \frac{1}{N_{mc}} \sum_{i=1}^{N_{mc}} I_G(\boldsymbol{\eta}; \mathbf{y} | \mathbf{S} = \mathbf{S}_i)$, where \mathbf{S}_i denotes the i th realization of \mathbf{S} and $N_{mc} = 5000$ represents the number of Monte-Carlo trails. The legend ‘Theo.’ denotes the theoretical result of the SMI given in (6). The legend ‘Upperbound’ denotes the upper bound in (5) and the legend ‘Lowerbound’ represents the lower bound of SMI given in *Proposition 2*. It can be observed that the approximation in (5) is very accurate, particularly when N_S is large. This validates *Proposition 1*. Meanwhile, a discrepancy consistently exists between SMI and its upper bound. As N_S decreases, this discrepancy becomes more obvious.

Fig. 2 compares the theoretical and simulation results with $N_S = 32$. We can observe that, as K increases, the discrepancy between the SMI and its upper bound becomes more pronounced. This is because the sensing DoF loss increases with the increasing of K . In this case, more samples are

¹Note that we simplify the notation by omitting the argument of $\mathbf{M}_{T,j}(\mathbf{F})$, $\alpha_j(\mathbf{F})$, $\mathbf{T}(\mathbf{F})$, and $\Delta'_{\lambda_{R,j}}(\mathbf{F})$ in (16).

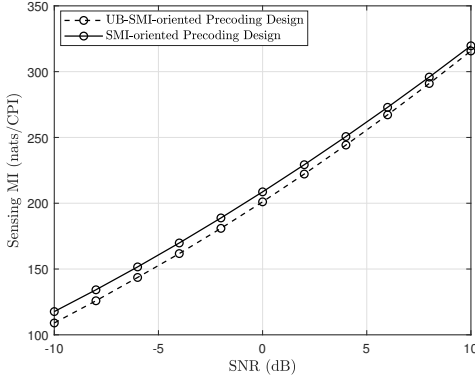


Fig. 3. Sensing MI versus SNR.

required to approach the upper bound of SMI, potentially leading to high latency.

B. Performance of the proposed manifold-based method

Note that, as $N_S \rightarrow \infty$, SMI will approach its upper bound (5). This allows us to utilize the upper bound as an approximation when N_S is large. However, when N_S is small, the approximation is not accurate. In Fig. 3, we compare the proposed method that maximizes the SMI in (6) and the method that optimizes the upper bound in (5). The legend ‘SMI-oriented Precoding Design’ denotes the SMI obtained by the proposed manifold-based method and the legend ‘UB-SMI-oriented Precoding Design’ represents the SMI obtained by the method given in [19], which maximizes (5). The number of frames and targets are set as $N_S = 32$ and $K = 15$, respectively. It can be observed from Fig. 3 that the proposed method outperforms the existing one, and the performance gap between the two methods becomes smaller as SNR increases.

VI. CONCLUSION

This paper investigated the achievable sensing performance and precoder design for ISAC systems utilizing random signals. For that purpose, we first derived the closed-form expression for SMI by utilizing random matrix theory. It was shown that the SMI with random signals is upper bounded by that with specific deterministic signals and SMI approaches its upper bound when the number of frames increases to infinity. Additionally, we analyzed the effect of the number of sensing frames and investigated the sensing DoF loss caused by random signals. Finally, a manifold-based optimization approach was proposed to maximize the SMI by designing the precoder. Simulation results validated the accuracy of the theoretical result and the effectiveness of the proposed precoder design method.

APPENDIX A PROOF OF PROPOSITION 1

This proof is equivalent to analyze the asymptotic behavior of the following random variable

$$\varrho = \log \left| \mathbf{I} + \sigma_N^{-2} \mathbf{R}_R \otimes (\mathbf{S}^H \mathbf{F}^H \mathbf{R}_T \mathbf{F} \mathbf{S}) \right|. \quad (20)$$

In fact, *Proposition 1* is an extension of [6, Theorems 1], which is summarized in the following lemma.

Lemma 1 ([6, Theorems 1]): Given two diagonal matrices \mathbf{D}_n and $\tilde{\mathbf{D}}_n$, we can define $\mathbf{Z}_n = \mathbf{D}_n^{\frac{1}{2}} \tilde{\mathbf{Z}}_n \tilde{\mathbf{D}}_n^{\frac{1}{2}}$, where $\tilde{\mathbf{Z}}_n$ has i.i.d. entries with distribution $\mathcal{CN}(0, \frac{1}{n})$. Then, we have

$$\mathbb{E} \log \left| \rho \mathbf{Z}_n \mathbf{Z}_n^H + \mathbf{I} \right| = V_n(\rho) + \mathcal{O} \left(\frac{1}{n} \right), \quad (21)$$

where

$$V_n(\rho) = \log \left| \mathbf{I} + \rho \delta_n(\rho) \tilde{\mathbf{D}}_n \right| + \log \left| \mathbf{I} + \rho \tilde{\delta}_n(\rho) \mathbf{D}_n \right| - n \rho \delta_n(\rho) \tilde{\delta}_n(\rho), \quad (22)$$

and $(\delta_n(\rho), \tilde{\delta}_n(\rho))$ is the unique positive solution of the following fixed-point equations

$$\begin{cases} \delta = \frac{1}{n} \text{tr} \mathbf{D}_n \left(\mathbf{I} + \rho \delta \mathbf{D}_n \right)^{-1} \\ \tilde{\delta} = \frac{1}{n} \text{tr} \tilde{\mathbf{D}}_n \left(\mathbf{I} + \rho \tilde{\delta} \tilde{\mathbf{D}}_n \right)^{-1} \end{cases}. \quad (23)$$

The main idea of this proof is to recast $I_G(\mathbf{h}; \mathbf{y} | \mathbf{S})$ into an extended model which fits into the framework of [6].

First, by utilizing the property of block diagonal matrix and the equality $\det(\mathbf{I} + \mathbf{A}\mathbf{B}) = \det(\mathbf{I} + \mathbf{B}\mathbf{A})$, (20) can be rewritten as $\varrho = \sum_{j=1}^K \varrho_j$, where $\varrho_j = \log \det \left(\mathbf{I}_{N_T} + \lambda_{R,j} \mathbf{R}_T^{\frac{1}{2}} \mathbf{F} \mathbf{S} \mathbf{S}^H \mathbf{F}^H \mathbf{R}_T^{\frac{1}{2}} \right)$. By performing the eigenvalue decomposition on $\mathbf{T} \triangleq \mathbf{R}_T^{\frac{1}{2}} \mathbf{F} \mathbf{F}^H \mathbf{R}_T^{\frac{1}{2}}$, we have $\mathbf{T} = \mathbf{U}_T \tilde{\mathbf{\Lambda}}_T \mathbf{U}_T^H$, where $\mathbf{U}_T \in \mathcal{C}^{N_T \times N_T}$ denotes the eigenvectors and

$$\tilde{\mathbf{\Lambda}}_T = \begin{bmatrix} \mathbf{\Lambda}_T & \mathbf{0} \\ \mathbf{0} & \mathbf{0} \end{bmatrix}, \quad (24)$$

with $\mathbf{\Lambda}_T \in \mathcal{C}^{K \times K}$ denotes the eigenvalue matrix.

Note that, with any unitary matrices \mathbf{U} and \mathbf{V} , the random matrices $\mathbf{U}\mathbf{S}\mathbf{V}$ and \mathbf{S} are statistically equivalent [6]. Thus, by omitting some constants independent of \mathbf{S} , the asymptotic behavior of ϱ_j is equivalent to that of the RV $\hat{\varrho}_j = \log \det \left(\mathbf{I}_K + \lambda_{R,j} \mathbf{\Lambda}_T^{\frac{1}{2}} \mathbf{S} \mathbf{S}^H \mathbf{\Lambda}_T^{\frac{1}{2}} \right)$.

By invoking $\mathbf{D}_n = \mathbf{\Lambda}_T$, $\tilde{\mathbf{D}}_n = \mathbf{I}_{N_S}$, $n = N_S$, and $\rho = \lambda_{R,j}$ into (23), we have $\tilde{\delta}(\rho) = 1/(1 + \rho\delta)$ such that the fixed-point equations in (23) reduce to a linear one with respect to δ , i.e.,

$$\delta(\rho) = \frac{1}{N_S} \text{tr} \mathbf{\Lambda}_T \left(\mathbf{I}_K + \frac{\rho}{1 + \rho\delta(\rho)} \mathbf{\Lambda}_T \right)^{-1}. \quad (25)$$

Furthermore, from *Lemma 1*, we can obtain that, as $N_S, N_T \rightarrow \infty$, one has

$$\mathbb{E}(\hat{\varrho}_j) = \bar{\varrho}_j + \mathcal{O} \left(\frac{1}{N_S} \right), j = 1, 2, \dots, \quad (26)$$

where

$$\begin{aligned} \bar{\varrho}_j = & \log \left| \mathbf{I}_K + \frac{\lambda_{R,j}}{1 + \lambda_{R,j} \delta(\lambda_{R,j})} \mathbf{\Lambda}_T \right| \\ & + N_S \log \left(1 + \lambda_{R,j} \delta(\lambda_{R,j}) \right) - \frac{N_S \lambda_{R,j} \delta(\lambda_{R,j})}{1 + \lambda_{R,j} \delta(\lambda_{R,j})}. \end{aligned} \quad (27)$$

Then, by utilizing the property of the unitary matrix \mathbf{U}_T , (27) and (25) are equivalent to (7) and (8), respectively, which completes the proof.

APPENDIX B
PROOF OF PROPOSITION 2

Since $\log(1+x) - \frac{x}{1+x} \geq 0$ for $x \geq 0$, we have

$$\begin{aligned} \bar{q}_j(\mathbf{F}) &\geq \log \left| \mathbf{I}_{N_T} + \frac{\lambda_{R,j}}{1 + \lambda_{R,j}\delta(\lambda_{R,j})} \mathbf{T}(\mathbf{F}) \right| \\ &\stackrel{(a)}{\geq} \frac{1}{1 + \lambda_{R,j}\delta(\lambda_{R,j})} \log |\mathbf{I}_{N_T} + \lambda_{R,j} \mathbf{T}(\mathbf{F})|, \end{aligned} \quad (28)$$

where step (a) follows the Jensen's inequality. Recalling (8), we have

$$\delta(\rho) = \frac{1}{N_S} \sum_{i=1}^{r_T} \lambda_{T,i} \left(1 + \frac{\rho}{1 + \rho\delta(\rho)} \lambda_{T,i} \right)^{-1}, \quad (29)$$

where $r_T = \text{rank}(\mathbf{T}) \leq \min\{K, \text{rank}(\mathbf{F}\mathbf{F}^H)\}$ and $\lambda_{T,i}$ denotes the i th non-zero eigenvalue of \mathbf{T} . Given $a > 0$, $\frac{x}{1+ax}$ is monotonically increasing for $x \geq 0$. Thus, we have

$$\delta(\rho) \leq \lim_{\lambda_{T,i} \rightarrow \infty} \delta(\rho) = \frac{r_T(1 + \rho\delta(\rho))}{\rho N_S}. \quad (30)$$

Given $N_S \geq K \geq r_T$, we have

$$\delta(\rho) \leq \frac{r_T}{\rho(N_S - r_T)}. \quad (31)$$

By substituting (31) into (28), we have

$$\bar{q}_j(\mathbf{F}) \geq \frac{N_S - r_T}{N_S} \log |\mathbf{I}_{N_T} + \lambda_{R,j} \mathbf{T}(\mathbf{F})|. \quad (32)$$

By taking the summation of (32) over index j , (12) can be obtained.

APPENDIX C
PROOF OF PROPOSITION 3

From (8), we have $\delta(\rho) = \frac{1}{N_S} \text{tr} \mathbf{T} \mathbf{M}_T$, where $\mathbf{M}_T(\rho) \triangleq (\mathbf{I}_{N_S} + \alpha(\rho) \mathbf{T})^{-1}$ and $\alpha(\rho) = \frac{\rho}{1 + \rho\delta(\rho)}$. The derivative of $\alpha(\rho)$ with respect to the (m, n) th entry of \mathbf{F} , denoted by $F_{m,n}^*$, is given by

$$\alpha'_{m,n}(\rho) = \frac{\partial \alpha(\rho)}{\partial F_{m,n}^*} = -\alpha^2(\rho) [\Delta'_\rho(\mathbf{F})]_{m,n}. \quad (33)$$

The derivative of \mathbf{T} with respect to $F_{m,n}^*$ can be expressed as

$$[\mathbf{T}']_{m,n} = \frac{\partial \mathbf{T}}{\partial F_{m,n}^*} = \mathbf{R}_T^{\frac{1}{2}} \mathbf{F} \mathbf{e}_n \mathbf{e}_m^T \mathbf{R}_T^{\frac{1}{2}}. \quad (34)$$

Therefore, we have

$$\begin{aligned} [\Delta'_\rho(\mathbf{F})]_{m,n} &= \frac{\partial \frac{1}{N_S} \text{tr} \mathbf{T} (\mathbf{I}_{N_S} + \alpha(\rho) \mathbf{T})^{-1}}{\partial F_{m,n}^*} \\ &= \frac{1}{N_S} \text{tr} [\mathbf{T}']_{m,n} \mathbf{M}_T(\rho) \\ &\quad - \frac{1}{N_S} \text{tr} \mathbf{T} \mathbf{M}_T(\rho) (\alpha'_{m,n}(\rho) \mathbf{T} + \alpha(\rho) [\mathbf{T}']_{m,n}) \mathbf{M}_T(\rho) \\ &= \frac{\alpha^2(\rho) \text{tr} (\mathbf{T} \mathbf{M}_T(\rho))^2}{N_S} [\Delta'_\rho(\mathbf{F})]_{m,n} + \frac{[\mathbf{R}_T^{\frac{1}{2}} \mathbf{M}_T^2(\rho) \mathbf{R}_T^{\frac{1}{2}} \mathbf{F}]_{m,n}}{N_S}. \end{aligned}$$

The solution to the above linear equation is given by

$$[\Delta'_\rho(\mathbf{F})]_{m,n} = \frac{[\mathbf{R}_T^{\frac{1}{2}} \mathbf{M}_T^2(\rho) \mathbf{R}_T^{\frac{1}{2}} \mathbf{F}]_{m,n}}{N_S - \alpha^2(\rho) \text{tr} (\mathbf{T}(\mathbf{F}) \mathbf{M}_T(\rho))^2}. \quad (35)$$

By consolidating all $[\Delta'_\rho(\mathbf{F})]_{m,n}$ into one matrix, we can obtain (15).

REFERENCES

- [1] F. Liu, Y. Cui, C. Masouros, J. Xu, T. X. Han, Y. C. Eldar, and S. Buzzi, "Integrated sensing and communications: Toward dual-functional wireless networks for 6g and beyond," *IEEE J. Sel. Areas Commun.*, vol. 40, no. 6, pp. 1728–1767, 2022.
- [2] L. Xie, S. Song, Y. C. Eldar, and K. B. Letaief, "Collaborative sensing in perceptive mobile networks: Opportunities and challenges," *IEEE Wirel. Commun.*, vol. 30, no. 1, pp. 16–23, 2023.
- [3] F. Liu, Y.-F. Liu, A. Li, C. Masouros, and Y. C. Eldar, "Cramér-rao bound optimization for joint radar-communication beamforming," *IEEE Trans. Signal Process.*, vol. 70, pp. 240–253, 2021.
- [4] L. Xie, P. Wang, S. Song, and K. B. Letaief, "Perceptive mobile network with distributed target monitoring terminals: Leaking communication energy for sensing," *IEEE Trans. Wirel. Commun.*, vol. 21, no. 12, pp. 10 193–10 207, 2022.
- [5] S. Herbert, J. R. Hoggood, and B. Mulgrew, "Mmse adaptive waveform design for active sensing with applications to mimo radar," *IEEE Trans. Signal Process.*, vol. 66, no. 5, pp. 1361–1373, 2017.
- [6] W. Hachem, O. Khorunzhiy, P. Loubaton, J. Najim, and L. Pastur, "A new approach for mutual information analysis of large dimensional multi-antenna channels," *IEEE Trans. Inf. Theory*, vol. 54, no. 9, pp. 3987–4004, 2008.
- [7] Y.-C. Ko, M.-S. Alouini, and M. K. Simon, "Outage probability of diversity systems over generalized fading channels," *IEEE Trans. commun.*, vol. 48, no. 11, pp. 1783–1787, 2000.
- [8] M. R. Bell, "Information theory and radar waveform design," *IEEE Trans. Inf. Theory*, vol. 39, no. 5, pp. 1578–1597, 1993.
- [9] B. Tang and J. Li, "Spectrally constrained mimo radar waveform design based on mutual information," *IEEE Trans. Signal Process.*, vol. 67, no. 3, pp. 821–834, 2018.
- [10] Y. Yang and R. S. Blum, "Mimo radar waveform design based on mutual information and minimum mean-square error estimation," *IEEE Trans. Aerosp. electro. syst.*, vol. 43, no. 1, pp. 330–343, 2007.
- [11] F. Liu, Y. Xiong, K. Wan, T. X. Han, and G. Caire, "Deterministic-random tradeoff of integrated sensing and communications in gaussian channels: A rate-distortion perspective," in *2023 IEEE International Symposium on Information Theory (ISIT)*. IEEE, 2023, pp. 2326–2331.
- [12] F. Dong, F. Liu, S. Lu, and Y. Xiong, "Rethinking estimation rate for wireless sensing: A rate-distortion perspective," *arXiv preprint arXiv:2303.11857*, 2023.
- [13] K. Yu, M. Bengtsson, B. Ottersten, D. McNamara, P. Karlsson, and M. Beach, "Second order statistics of nlos indoor mimo channels based on 5.2 ghz measurements," in *GLOBECOM'01. IEEE Global Telecommunications Conference (Cat. No.01CH37270)*, vol. 1, 2001, pp. 156–160 vol.1.
- [14] J. Kermaol, L. Schumacher, K. Pedersen, P. Mogensen, and F. Frederiksen, "A stochastic mimo radio channel model with experimental validation," *IEEE J. Sel. Areas Commun.*, vol. 20, no. 6, pp. 1211–1226, 2002.
- [15] K. Yu, M. Bengtsson, B. Ottersten, D. McNamara, P. Karlsson, and M. Beach, "Modeling of wide-band mimo radio channels based on nlos indoor measurements," *IEEE Trans. Veh. Technol.*, vol. 53, no. 3, pp. 655–665, 2004.
- [16] Z. Ren, Y. Peng, X. Song, Y. Fang, L. Qiu, L. Liu, D. W. K. Ng, and J. Xu, "Fundamental crb-rate tradeoff in multi-antenna isac systems with information multicasting and multi-target sensing," *IEEE Trans. Wirel. Commun.*, 2023.
- [17] Y. Xiong, F. Liu, Y. Cui, W. Yuan, T. X. Han, and G. Caire, "On the fundamental tradeoff of integrated sensing and communications under gaussian channels," *IEEE Trans. Inf. Theory*, 2023.
- [18] P.-A. Absil, R. Mahony, and R. Sepulchre, *Optimization algorithms on matrix manifolds*. Princeton University Press, 2008.
- [19] M. Biguesh and A. B. Gershman, "Training-based mimo channel estimation: A study of estimator tradeoffs and optimal training signals," *IEEE trans. signal process.*, vol. 54, no. 3, pp. 884–893, 2006.